A COMPARISON OF SPLITTING TECHNIQUES FOR 3D FFD MIGRATION

J.C. Costa, D. Mondini, J. Schleicher, and A. Novais

email: *jesse@ufpa.br*
keywords: *Wave-equation migration, two-way splitting, FFD*

ABSTRACT

Three-dimensional wave-equation migration techniques are still quite expensive because of the huge matrices that need to be inverted. Several techniques have been proposed to reduce this cost by splitting the full 3D problem into a sequence of 2D problems. We compare the performance of splitting techniques for stable 3D Fourier Finite-Difference (FFD) migration techniques in terms of image quality and computational cost. The FFD methods are complex Padé FFD and FFD plus interpolation, and the compared splitting techniques are two and four-way splitting as well as alternating four-way splitting, i.e., splitting into the coordinate directions at one depth and the diagonal directions at the next depth level. From numerical examples in homogeneous and inhomogeneous media, we conclude that alternate four-way splitting yields results of the same quality as full four-way splitting at the cost of two-way splitting.

INTRODUCTION

Because of its superiority in areas of complex geology, wave-equation migration is substituting Kirchhoff migration in practice. However, while Kirchhoff migration counts on more than 30 years of technological development, wave-equation migration methods still need to be improved in various aspects. One of these aspects is the efficient implementation of three-dimensional wave-equation migration.

The application of a three-dimensional wave-equation migration technique adds the problem of computational cost to those of stability and precision of the chosen migration algorithm. To speed up migration techniques like finite-difference (FD) (Claerbout, 1971) or Fourier finite-difference (FFD) migration (Ristow and Rühl, 1994), a technique known as splitting is frequently used. In this context, splitting means the separation of a single-step 3D migration into two 2D passes within planes parallel to the horizontal coordinate axes, usually the inline and crossline directions (Brown, 1983).

When the splitting is applied to the implicit FD migration operator in such a way that the resulting equations are solved alternatingly in the inline and crossline directions, the resulting FD scheme is known as an Alternating-Direction-Implicit (ADI) scheme. This procedure has the drawback of being incorrect for strongly dipping reflectors, resulting in large positioning errors for this type of reflectors when the dip direction is away from the coordinate directions and thus outside the migration planes. This imprecision leads to numerical anisotropy, i.e., a migration operator that acts quite differently in different directions.

To improve this behaviour while retaining the advantages of a rather low computation cost, different procedures have been proposed over the years. Ristow (1980, see also Ristow and Rühl, 1997) proposed to perform, in addition to the 2D migration in the coordinate planes, also 2D migrations in the diagonal directions between the coordinate axes. Kitchenside (1988) used phase-shift migration plus an additional FD propagation step of the residual field to reduce the splitting error. Graves and Clayton (1990) proposed the implementation of a phase-correction operator using FD and incorporating a damping function to guarantee the stability of the 3D FD migration scheme.

Inverting the idea of Kitchenside (1988), who propagated the field using phase shift and the residual using FD, Li (1991) proposed to use conventional FD migration plus a residual field correction by phase shift to improve the migrated image quality. Without any need to modify the conventional 3D FD migration, the Li correction adds a phase-shift filter at certain steps of the downward extrapolation. This technique corrects not only for the splitting error, but also for the positioning error of steeply dipping reflectors.

Collino and Joly (1995) solved a family of new 3D one-way wave equations by the ADI method. These equations significantly reduce the numerical anisotropy, but are approximately four times as expensive as conventional two-way splitting. Wang (2001) developed an alternative method to improve the precision of the FD solution of the one-way wave equation. To guarantee stability and efficiency, he keeps the implicit FD scheme and the alternation of directions, but interpolates between the ADI solution and the wavefield before each step of extrapolation. He calls the resulting method ADI plus interpolation (ADIPI). As a drawback, this ADIPI can produce instabilities in the presence of strong lateral velocity variations.

Zhou and McMechan (1997) proposed a $45°$ one-way wave equation that can be expressed as a system of differential equations of first and second order (Zhang et al., 1988), and factored into a product of two one-dimensional terms corresponding to the lateral directions (Mitchell and Griffiths, 1980; Graves and Clayton, 1990). A big asset of the method is that the conventional FD extrapolation can be used with very little modification. In this way, the efficiency of conventional splitting is preserved, without adding the necessity of any error compensation. However, the method is also instable for strong lateral velocity contrasts and needs rather heavy model smoothing.

Biondi (2002) showed that FFD migration is more precise than other methods that use implicit finite differences like pseudoscreen propagators (Jin et al., 1999) and high-angle screen propagators (Xie and Wu, 1998). Given that the computational complexity of all three methods is approximately the same, FFD migration is more attractive than the others. Unfortunately, when conventional FFD migration is applied in the presence of strong velocity contrasts, it can generate numerical instabilities, too.

To overcome the problem of instabilities in models with strong lateral velocity contrasts, Biondi (2002) presented a correction to the FFD method that avoids stability problems. To derive it, he adapted a theory of Godfrey et al. (1979) and Brown (1979), which improves the stability of the $45°$ equation. The corrected FFD method is unconditionally stable for arbitrary velocity variations, as much in the velocity model as in the reference velocity. Particularly, and differently from conventional FFD migration, it is unconditionally stable even if the reference velocity is smaller than the model velocity. This new property allows for the application of the interpolation technique, conventionally used to improve phase-shift and split-step migration (Gazdag and Sguazzero, 1984) but impossible in FFD migration, because it needs propagation with a larger and a smaller reference velocity. The resulting migration technique is called FFD plus interpolation, or shortly FFDPI.

Another, computationally less expensive method to stabilize FFD migration in the presence of strong lateral velocity contrasts was proposed by Amazonas et al. (2007). It substitutes the real Padé approximation (Bamberger et al., 1988) used in the derivation of FFD migration (Ristow and Rühl, 1994) by its complex version (Millinazzo et al., 1997). In this way, the incorrect treatment of near horizontal and slightly evanescent waves of the real Páde approximation is improved, leading to a more stable FFD algorithm, shortly referred to as complex Padé FFD (CPFFD) migration.

In this work, we study possibilities of efficiently implementing these stable FFD migration techniques in 3D. We implemented and compared splitting techniques for FFDPI (Biondi, 2002) and CPFFD (Amazonas et al., 2007) migration. Our numerical tests indicate that a very robust, highly efficient, and satisfactorily accurate method is alternate four-way splitting, i.e., splitting into the coordinate directions at one extrapolation step and into the diagonal directions at the next step.

THEORETICAL BACKGROUND

The one-way wave equation

The one-way wave equation (Leontovich and Fock, 1946) can be derived starting from the scalar wave equation, which for a homogeneous medium is given by

$$\frac{\partial^2 p(\mathbf{x}, t)}{\partial z^2} + \frac{\partial^2 p(\mathbf{x}, t)}{\partial x^2} + \frac{\partial^2 p(\mathbf{x}, t)}{\partial y^2} - \frac{1}{c^2} \frac{\partial^2 p(\mathbf{x}, t)}{\partial t^2} = 0 \,, \tag{1}$$

where $p(\mathbf{x}, t)$ is the scalar wavefield and $c = c(\mathbf{x})$ is the spatially varying wave velocity. For moderately varying media, where velocity derivatives can be neglected, Fourier transform in time and horizontal coordinates x and y allows to represent equation (1) as

$$\frac{\partial^2 P(k_x, k_y, z, \omega)}{\partial z^2} - \frac{(-i\omega)^2}{c^2}\left(1 - \frac{c^2}{\omega^2}(k_x^2 + k_y^2)\right)P(k_x, k_y, z, \omega) = 0 \ . \tag{2}$$

Equation (2) can be factorized into

$$\left[\frac{\partial P(k_x, k_y, z, \omega)}{\partial z} - \frac{(-i\omega)}{c}\sqrt{1 - \frac{c^2}{\omega^2}(k_x^2 + k_y^2)}\right] \times$$
$$\left[\frac{\partial P(y, k_x, \omega)}{\partial z} + \frac{(-i\omega)}{c}\sqrt{1 - \frac{c^2}{\omega^2}(k_x^2 + k_y^2)}\right] P(k_x, k_y, z, \omega) = 0 \ . \tag{3}$$

The two differential operators in equation (3) represent, when taken alone, one-way wave equations that describe up and downgoing waves. For migration, the one-way wave equation of interest is the one describing downgoing waves, i.e.,

$$\frac{\partial P(k_x, k_y, z, \omega)}{\partial z} = \frac{(-i\omega)}{c}\sqrt{1 - \frac{c^2}{\omega^2}(k_x^2 + k_y^2)}P(k_x, k_y, z, , \omega) \ . \tag{4}$$

Inverse Fourier transform in the horizontal wavenumbers k_x and k_y yields then formally

$$\frac{\partial P(\mathbf{x}, \omega)}{\partial z} = \frac{(-i\omega)}{c(\mathbf{x})}\sqrt{1 + \frac{c^2(\mathbf{x})}{\omega^2}\left(\frac{\partial^2}{\partial x^2} + \frac{\partial^2}{\partial y^2}\right)} P(\mathbf{x}, \omega) \ . \tag{5}$$

The actual restrictions that apply to equation (5) in inhomogeneous media are much less severe than the above derivation indicates. Of course, for the formal representation (5) to make practical sense, the square root of the differential operator needs to be approximated in terms of numerically executable operations.

Expansion of the square root

A well-used possibility for the approximation of the square root in the one-way wave equation (5) in terms of numerically executable operations is an expansion into a Padé series (Bamberger et al., 1988)

$$\sqrt{1 + Z} \approx 1 + \sum_{n=1}^{N} \frac{a_n Z}{1 + b_n Z} \tag{6}$$

where the Padé coefficients are

$$a_n = \frac{2}{2N + 1}\sin^2\left(\frac{n\pi}{2N + 1}\right) \ , \qquad \text{and} \qquad b_n = \cos^2\left(\frac{n\pi}{2N + 1}\right) \ . \tag{7}$$

This approximation is used in most practical FD migration schemes. Depending on the number N of terms used in the expansion, it gives rise to the so-called $15°$, $45°$, or $60°$ migrations.

However, when the interest is on accurate imaging up to very high propagation angles, approximation (6) has a drawback. For propagation angles close to $90°$, the argument Z of equation (6) becomes close to -1. However, for $Z < -1$, where wave propagation enters the evanescent domain, the left side of equation (6) is imaginary, while its right side remains real. Thus, the approximation breaks down abruptly, which causes instabilities when using the real approximation (6) for migration in models with strong lateral velocity contrasts.

To overcome this problem, Millinazzo et al. (1997) proposed to rotate the branch cut of the complex plane before application of the Padé approximation. Denoting the rotation angle by α, the representation of the square root is

$$\sqrt{1 + Z} = e^{i\alpha/2}\sqrt{(1 + Z)e^{-i\alpha}} = e^{i\alpha/2}\sqrt{1 + [(1 + Z)e^{-i\alpha} - 1]} \ , \tag{8}$$

which, after expansion into a Padé series according to equation (6), yields

$$\sqrt{1 + Z} = C_0 + \sum_{n=1}^{N} \frac{A_n Z}{1 + B_n Z} \ , \tag{9}$$

where the complex Padé coefficients are given by

$$A_n \ \equiv \ \frac{a_n e^{-i\alpha/2}}{[1 + b_n(e^{-i\alpha} - 1)]^2} \ , \qquad\qquad B_n \ \equiv \ \frac{b_n e^{-i\alpha}}{1 + b_n(e^{-i\alpha} - 1)} \ , \tag{10}$$

$$C_0 \ \equiv \ e^{i\alpha/2} \left\{ 1 + \sum_{n=1}^{N} \frac{a_n(e^{-i\alpha} - 1)}{[1 + b_n(e^{-i\alpha} - 1)]} \right\} \ . \tag{11}$$

Note that in equation (11), C_0 is an approximation to one. This approximation gets the better the more terms N are used in the sum. However, for a finite number of terms N, this approximation is always imperfect. Therefore, it is more practical to directly use $C_0 = 1$. We will use this value for C_0 in the following derivations.

Fourier finite difference migration

The complex Padé approximation (9) allows more stable implementations of not only FD but also FFD migration (Amazonas et al., 2007). The derivation of 3D complex Padé FFD (CPFFD) migration is very similar to the original derivation of Ristow and Rühl (1994). It starts from the difference between the square root of equation (5) and a corresponding one where the velocity has been replaced by a constant reference velocity c_r, viz.,

$$\frac{i\omega}{c(\mathbf{x})} \sqrt{1 + \left(\frac{c(\mathbf{x})}{\omega}\right)^2 \left(\frac{\partial^2}{\partial x^2} + \frac{\partial^2}{\partial y^2}\right)} - \frac{i\omega}{c_r} \sqrt{1 + \left(\frac{c_r}{\omega}\right)^2 \left(\frac{\partial^2}{\partial x^2} + \frac{\partial^2}{\partial y^2}\right)} \ . \tag{12}$$

Expanding both square roots in equation (12) in complex Padé series according to equation (9), we find

$$ik_0 \left\{ p\sqrt{1 + X^2} - \sqrt{1 + p^2 X^2} \right\} \approx ik_0 \left\{ p \left[1 + \sum_{n=1}^{N} \frac{A_n X^2}{1 + B_n X^2} \right] - \left[1 + \sum_{n=1}^{N} \frac{A_n p^2 X^2}{1 + B_n p^2 X^2} \right] \right\} \ , \tag{13}$$

where we have used the notations

$$k_0 \equiv \frac{\omega}{c_r} \ , \qquad p \equiv \frac{c_r}{c(\mathbf{x})} \ , \qquad \text{and} \qquad X^2 \equiv \left(\frac{c(\mathbf{x})}{\omega}\right)^2 \left(\frac{\partial^2}{\partial x^2} + \frac{\partial^2}{\partial y^2}\right) \ . \tag{14}$$

Joining the two series into one, expanding the fractions into Taylor series, and grouping the terms of equal power leads to

$$ik_0 \left\{ p\sqrt{1 + X^2} - \sqrt{1 + p^2 X^2} \right\} \approx ik_0 \bigg\{ p - 1$$
$$+ \left[\sum_{n=1}^{N} A_n p(1 - p)X^2 \left(1 - B_n \frac{(1-p^3)}{1-p} X^2 + B_n^2 \frac{(1-p^5)}{1-p} X^4 - B_n^3 \frac{(1-p^7)}{1-p} X^6 + ... \right) \right] \bigg\} \ . \tag{15}$$

Since

$$\frac{1 - p^{n+1}}{1 - p} = 1 + p + p^2 + ... + p^n \ , \tag{16}$$

this expression is, up to second order, equivalent to a Taylor series expansion of a Padé expression of the form

$$ik_0 \left\{ p\sqrt{1 + X^2} - \sqrt{1 + p^2 X^2} \right\} \approx ik_0 \bigg\{ (p - 1) + \sum_{n=1}^{N} \frac{A_n p(1 - p)X^2}{1 + \sigma B_n X^2} \bigg\} \ , \tag{17}$$

where $\sigma = 1 + p + p^2$.

Using this approximation, the one-way wave equation (5) can be represented as

$$\frac{dP}{dz} = \left\{ -ik_0\sqrt{1 + p^2X^2} - ik_0\left[(p-1) + \sum_{n=1}^{N} \frac{A_n p(1-p)X^2}{1 + B_n\sigma X^2} \right] \right\} P \,, \tag{18}$$

which is the complex Padé equivalent to standard FFD migration (Ristow and Rühl, 1994).

As seen above, the theoretical value of σ obtained from this expansion is $\sigma = 1 + p + p^2$. However, 2D numerical experiments of Amazonas et al. (2007) indicate that other expressions for σ can produce better results. For small contrasts, they suggest $\sigma = 3p$ and for high fidelity up to high propagation angles, they propose $\sigma = 1 + p^3$.

Implementation

To solve equation (18), we separate it into a set of differential equations. The first two terms provide the equations

$$\frac{dP}{dz} = -ik_0\sqrt{1 + p^2X^2}P \tag{19}$$

and

$$\frac{dP}{dz} = -ik_0(p-1) \,, \tag{20}$$

the analytic solutions of which are

$$P(x, z + \Delta z, \omega) = e^{-ik_0\sqrt{1+p^2X^2}\Delta z} P(x, z, \omega) \tag{21}$$

and

$$P(x, z + \Delta z, \omega) = e^{-ik_0\Delta z C_0(p-1)} P(x, z, \omega) \,. \tag{22}$$

The remaining terms of equation (18) from the Padé series are represented by differential equations

$$\frac{dP}{dz} = -ik_0\frac{A_n p(1-p)X^2}{1 + B_n\sigma X^2}P \,, \qquad (n = 1, \dots, N) \,. \tag{23}$$

Discretizing these differential equations using a Crank-Nicolson FD scheme, we obtain

$$\frac{P^{j+1} - P^j}{\Delta z} = -ik_0\frac{A_n p(1-p)X^2}{1 + B_n\sigma X^2}\frac{P^{j+1} + P^j}{2} \,, \tag{24}$$

where $P^j = P(\mathbf{r}, z_j, \omega)$. Equation (24) means that the following implicit equation needs to be solved:

$$\left\{ 1 + \left[B_n\sigma + i\frac{k_0\Delta z}{2}A_n p(1-p) \right] X^2 \right\} P^{j+1} = \left\{ 1 + \left[B_n\sigma - i\frac{k_0\Delta z}{2}A_n p(1-p) \right] X^2 \right\} P^j \,. \tag{25}$$

We still need to discretize of the derivatives in the horizontal coordinates, i.e., replace the differential operator X^2 by its difference operator

$$X^2 \approx \mathbf{X}^2 = \frac{c^2(x_k, y_l, z_j)}{\omega^2}\left(\frac{\mathbf{D}_x^2}{\Delta x^2} + \frac{\mathbf{D}_y^2}{\Delta y^2} \right) \,, \tag{26}$$

where the matrices $\mathbf{D}_x^2$ e $\mathbf{D}_y^2$ represent difference operators for the second derivatives in x and y. For simplicity, we choose second-order difference operators, i.e.,

$$\mathbf{D}_x^2 P_{k,l}^j = P_{k+1,l}^j - 2P_{k,l}^j + P_{k-1,l}^j \qquad \text{and} \qquad \mathbf{D}_y^2 P_{k,l}^j = P_{k,l+1}^j - 2P_{k,l}^j + P_{k,l-1}^j \,, \tag{27}$$

for $k = 1, \dots, n_x$ and $l = 1, \dots, n_y$ with n_x e n_y denoting the number of grid points in the x and y directions. The resulting difference equation equivalent to differential equation (23) reads

$$\left[\mathbf{I} + \mathbf{C}_n\left(\frac{\mathbf{D}_x^2}{\Delta x^2} + \frac{\mathbf{D}_y^2}{\Delta y^2} \right) \right] \mathbf{P}^{j+1} = \left[\mathbf{I} + \mathbf{C}_n^*\left(\frac{\mathbf{D}_x^2}{\Delta x^2} + \frac{\mathbf{D}_y^2}{\Delta y^2} \right) \right] \mathbf{P}^j \,, \tag{28}$$

where $\mathbf{I}$ is the identity matrix and $\mathbf{P}^j$ is the matrix formed by the elements $P_{k,l}^j$ at a fixed depth level z_j. Moreover, $\mathbf{C}_n$ is the complex matrix with elements

$$(\mathbf{C}_n)_{k,l} = \frac{c^2}{\omega^2}\left[B_n\sigma + i\frac{k_0\Delta z}{2}A_np(1-p)\right] ,\tag{29}$$

with $c = c(x_k, y_l, z_j)$, $\sigma = \sigma(x_k, y_l, z_j)$, and $p = p(x_k, y_l, z_j)$, and the asterisk denotes the complex conjugate.

Two-way splitting

In the technique called two-way splitting, also known as alternating-directions-implicit (ADI) method (Wachspress and Harbetler, 1960; Douglas, 1962; Mitchell and Griffiths, 1980), one substitutes equation (28) by its approximate factorized form

$$\left(\mathbf{I} + C_n\frac{\mathbf{D}_x^2}{\Delta x^2}\right)\left(\mathbf{I} + C_n\frac{\mathbf{D}_y^2}{\Delta y^2}\right)\mathbf{P}^{j+1} = \left(\mathbf{I} + C_n^*\frac{\mathbf{D}_x^2}{\Delta x^2}\right)\left(\mathbf{I} + C_n^*\frac{\mathbf{D}_y^2}{\Delta y^2}\right)\mathbf{P}^j .\tag{30}$$

This equation has the advantage of being solvable in two 2D steps. Under the assumption that the inverse operator in y, $\left(\mathbf{I} + C_n\mathbf{D}_y^2/\Delta y^2\right)^{-1}$, commutes with both operators in x, equation (30) can be rewritten as

$$\left(\mathbf{I} + C_n\frac{\mathbf{D}_x^2}{\Delta x^2}\right)\mathbf{P}^{j+1} = \left(\mathbf{I} + C_n^*\frac{\mathbf{D}_x^2}{\Delta x^2}\right)\tilde{\mathbf{P}}^j\tag{31}$$

where the intermediate value $\tilde{P}^j$, defined as

$$\tilde{\mathbf{P}}^j = \left(\mathbf{I} + C_n\frac{\mathbf{D}_y^2}{\Delta y^2}\right)^{-1}\left(\mathbf{I} + C_n^*\frac{\mathbf{D}_y^2}{\Delta y^2}\right)\mathbf{P}^j ,\tag{32}$$

can be found solving the system

$$\left(\mathbf{I} + C_n\frac{\mathbf{D}_y^2}{\Delta y^2}\right)\tilde{\mathbf{P}}^j = \left(\mathbf{I} + C_n^*\frac{\mathbf{D}_y^2}{\Delta y^2}\right)\mathbf{P}^j .\tag{33}$$

The advantage of splitting is in the computational cost. While the numerical solution of equation (28) requires the solution of a system of size $n_x \times n_y$, the cascaded solution of equations (33) and (31) demands only the solution of n_x systems of size n_y, followed by n_y systems of size n_x. Since all these systems are tridiagonal, there are very efficient ways to solve them, which makes the splitting technique orders of magnitude faster than the solution of the original 3D system.

On the other hand, this procedure also has disadvantages. The biggest one is the introduction of numerical anisotropy into the propagation of the wavefield, because the numerical error increases with the azimuth between the propagation direction and the coordinate directions. This degrades the migrated image, introducing errors in the positioning of steeply dipping reflectors.

Splitting in more directions

To overcome the problems with numerical anisotropy, Ristow and Rühl (1997) proposed to generalize the technique to splitting into more than two directions. The idea is to approximate the 3D square-root operator by a sequence of 2D operators in different directions. In practice, most uses rely on three, four or six directions to avoid symmetry problems. The unknown coefficients of these 2D operators are obtained from Taylor series expansions or by optimization techniques.

The multi-way splitting form of the 2D Padé operators is given by the complex Padé expansion of the square-root operator in equation (5) for multiple directions,

$$\sqrt{1 + \frac{c^2(\mathbf{x})}{\omega^2}\left(\frac{\partial^2}{\partial x^2} + \frac{\partial^2}{\partial y^2}\right)} \approx 1 + \frac{2}{K}\sum_{j=1}^{K}\sum_{n=1}^{N}\frac{\alpha_n w_j^2}{1 + \beta_n w_j^2} ,\tag{34}$$

where K is the number of directions. Moreover, w_j are the derivative operators in the splitting directions, i.e., $w_j = \cos \phi_j \, u + \sin \phi_j \, v$, with $\phi_j = (j-1)\Delta\phi$ (for $j = 1, 2, \ldots, K$, and $\Delta\phi = 2\pi/K$) being the azimuth of the rotated direction.

There are two ways of obtaining the unknown coefficients α_n and β_n in equation (34). One way is, as detailed above for the full 3D case, by Taylor series expansion of the fractions and comparison of the result with the direct Taylor series expansion of the square root. Alternatively, optimization techniques can be employed to find optimum coefficients that minimize the numerical anisotropy for a certain range of medium velocities and a given reference velocity within the range of interest of propagation angles.

In conventional implementations of multi-way splitting, operators (34) are applied in sequence at one single depth level before proceeding to the next one. In this paper, we apply the differential operators w_1 and w_3 for $\phi_1 = 0°$ and $\phi_3 = 90°$, i.e., the derivatives in the x and y directions, at one depth level, and leave the application of the operators w_2 and w_4 for $\phi_2 = 45°$ and $\phi_4 = 135°$, i.e., the derivatives in the diagonal directions, to the next depth level. In this way, we simulate four-way splitting, but with practically the same cost as conventional two-way splitting.

Stable FFD migration and FFDPI migration

We compare our results of CPFFD migration to another stable FFD migration technique, FFDPI migration (Biondi, 2002). It is based on a a correction to the FFD method that avoids stability problems. To derive it Biondi (2002) starts from the real version of equation (18). In our notation, he rewrites the last part of the operator inside the summation as

$$\frac{a_n p(1-p)X^2}{1 + b_n \sigma X^2} = \frac{a_n p(1-p)}{b_n \sigma} \frac{b_n \sigma X^2}{1 + b_n \sigma X^2} \, . \tag{35}$$

This representation of the operator corresponds to the differential equations

$$\frac{dP}{dz} = -ik_0 \frac{a_n p(1-p)}{b_n \sigma} \frac{b_n \sigma X^2}{1 + b_n \sigma X^2} P \, , \qquad (n = 1, \ldots, N) \, . \tag{36}$$

This form of the differential equation can be implemented in a stable way by the realization of the product σX^2 as a symmetrical matrix product $\mathbf{\Sigma}^T \mathbf{X}^2 \mathbf{\Sigma}$, where $\mathbf{\Sigma}$ is a diagonal matrix containing the values of the square root of σ. The remaining factor $a_n p(1-p)/b_n \sigma$ can also be represented as a product with a diagonal matrix.

In 3D, after two-way splitting, the resulting difference equation is approximated by the system

$$\left[\mathbf{I} + \mathbf{C}_x \mathbf{\Sigma}_x^T \mathbf{D}_x^2 \mathbf{\Sigma}_x\right] \mathbf{P}^{j+1} = \left[\mathbf{I} + \mathbf{C}_x^* \mathbf{\Sigma}_x^T \mathbf{D}_x^2 \mathbf{\Sigma}_x\right] \tilde{\mathbf{P}}^j \tag{37}$$

$$\left[\mathbf{I} + \mathbf{C}_y \mathbf{\Sigma}_y^T \mathbf{D}_y^2 \mathbf{\Sigma}_y\right] \tilde{\mathbf{P}}^j = \left[\mathbf{I} + \mathbf{C}_y^* \mathbf{\Sigma}_y^T \mathbf{D}_y^2 \mathbf{\Sigma}_y\right] \mathbf{P}^j \, , \tag{38}$$

where $\mathbf{\Sigma}_x$ and $\mathbf{\Sigma}_y$ are diagonal matrices with elements

$$(\mathbf{\Sigma}_x)_{km} = \frac{c(x_k, y_l, z_j)}{\omega \Delta x} \sqrt{b_n \sigma(x_k, y_l, z_j)} \delta_{km} \tag{39}$$

$$(\mathbf{\Sigma}_y)_{lm} = \frac{c(x_k, y_l, z_j)}{\omega \Delta y} \sqrt{b_n \sigma(x_k, y_l, z_j)} \delta_{lm} \, . \tag{40}$$

Moreover, matrices $\mathbf{C}_x$ e $\mathbf{C}_y$ are given by

$$\mathbf{C}_x = \mathbf{I} + i\frac{k_0 \Delta z}{2} \varepsilon \mathbf{\Delta}_x \qquad \text{and} \qquad \mathbf{C}_y = \mathbf{I} + i\frac{k_0 \Delta z}{2} \varepsilon \mathbf{\Delta}_y \, , \tag{41}$$

where $\mathbf{\Delta}_x$ and $\mathbf{\Delta}_y$ are diagonal matrices with elements

$$(\mathbf{\Delta}_x)_{km} = \frac{a_n}{b_n} \frac{p(x_k, y_l, z_j)|1 - p(x_k, y_l, z_j)|}{\sigma(x_k, y_l, z_j)} \delta_{km} \, , \tag{42}$$

$$(\mathbf{\Delta}_y)_{lm} = \frac{a_n}{b_n} \frac{p(x_k, y_l, z_j)|1 - p(x_k, y_l, z_j)|}{\sigma(x_k, y_l, z_j)} \delta_{lm} \, , \tag{43}$$

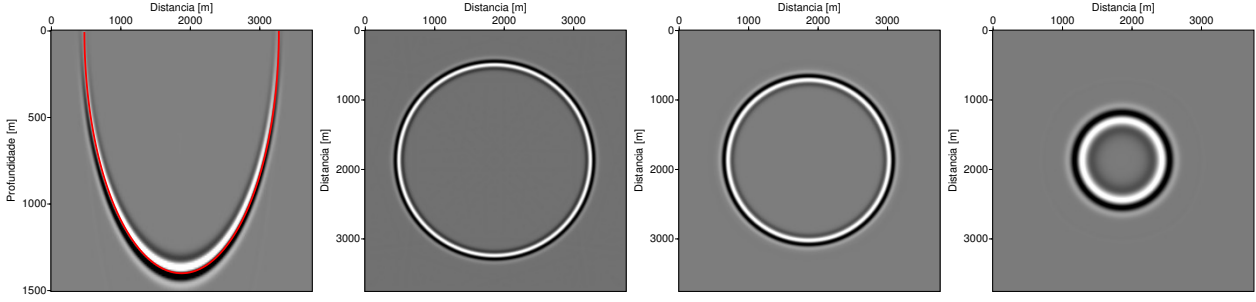and ε is given by

Figure 1: Reference impulse response, obtained with phase-shift migration using the true medium velocity. From left to right: Central vertical cut in the x-z plane, and horizontal cuts at 150 m, 750 m, and 1250 m depth.

$$\varepsilon = \mathrm{sgn}\,(1-p) = \left\{ \begin{array}{ll} 1 & \text{se } c_r < c(\mathbf{x})\,, \\ -1 & \text{se } c_r > c(\mathbf{x})\,. \end{array} \right. \tag{44}$$

According do Biondi (2002), for the equivalence between the original differential equation and its stable discretization to be guaranteed, it is essential that ε is constant on the depth level z_j under consideration, i.e., that the reference velocity is larger or smaller than all model velocities at the current depth level.

Biondi (2002) proves that this implementational correction stabilizes FFD migration, even in the presence of strong lateral velocity contrasts and for reference velocities larger than the medium velocity. In this way, this version of the FFD method possesses the necessary characteristics to be utilized as the main part of a precise and efficient high-angle wave-equation migration method. To attain a desired precision, one can interpolate between wavefields obtained for a sufficiently dense set of reference velocities. Theoretically, this allows to obtain arbitrary precision by increasing the number of reference velocities. The structure of this FFDPI method is similar to PSPI (Gazdag and Sguazzero, 1984) and to the extended split-step method (Kessinger, 1992).

NUMERICAL EXPERIMENTS

Tests in a homogeneous medium

To study the numerical anisotropy of FFD migration operators after splitting, we calculated impulse-responses for zero-offset migration in a homogeneous medium with velocity 2.5 km/s. The source pulse was a Ricker wavelet with central frequency 25 Hz, with its centre positioned at an arrival time of 0.56 s. The migration grid was $\Delta x = \Delta y = 12.5$ m, and $\Delta z = 10$ m. All our examples used a complex Padé implementation of FFD migration with 3 terms in the series.

Figure 1 shows one vertical and three horizontal cuts through the reference impulse response, obtained with phase-shift migration using the true medium velocity. The amplitude decay at high propagation angles is caused by the source implementation, which did not use the amplitude correction of Wapenaar (1990). The red line in the top left figure indicates the true theoretical position of the event, given by the half-circle $z = \sqrt{(ct_e)^2 - (x - x_s)^2}$, where t_e is the observation time of the event in the data, here 0.56 s, and x_s is the source position, here the centre of the image, i.e., $x_s = 1850$ m. The non-circular appearance of this line in Figure 1 is due to the overstretched vertical axis. For a better comparison, we will present all other impulse responses below in the same way.

Figure 2 shows the corresponding four cuts of the impulse response of complex Padé FFD migration using conventional two-way splitting. Here, the value of the reference velocity was chosen as $c_r = 1875$ m/s, i.e., $p = c_r/c(\mathbf{x}) = 0.75$. We observe the well-preserved circular shape of the impulse response in the deepest horizontal cut (bottom left), i.e., for propagation directions close to the vertical axis. However, the shallow and, principally, medium horizontal cuts reveal a visible deformation, indicating the loss of quality for higher propagation angles. Also note the amplitude loss in the directions of the coordinate axes that are visible in the shallow and medium horizontal cuts. In the vertical cut (top left), only a slight deformation from circular shape is visible, which is due to the cut being within the coordinate plane, where the errors are the smallest. The amplitude loss for high propagation angles reflects the quality of the three-term
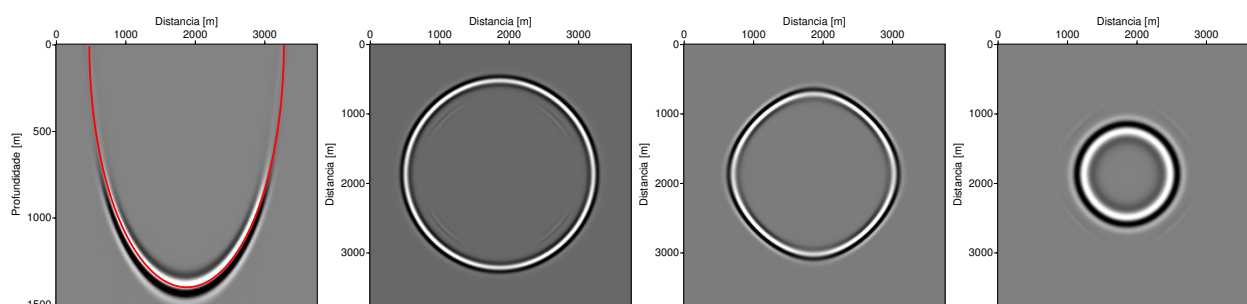
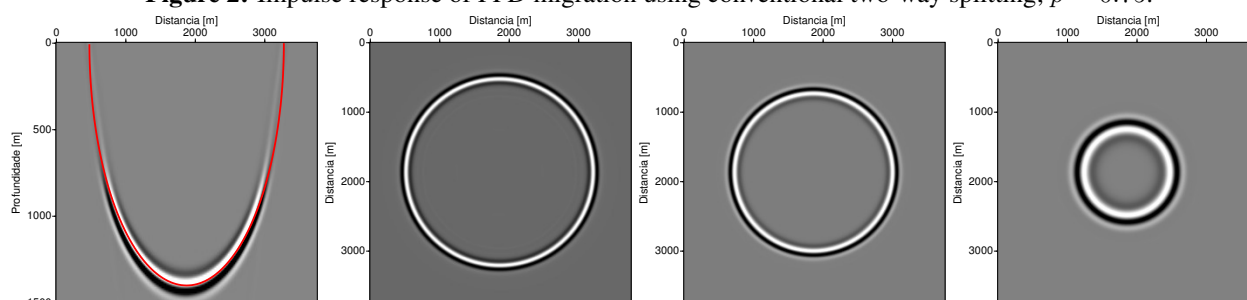**Figure 2:** Impulse response of FFD migration using conventional two-way splitting; $p = 0.75$.

Figure 3: Impulse response of FFD migration using conventional four-way splitting; $p = 0.75$.
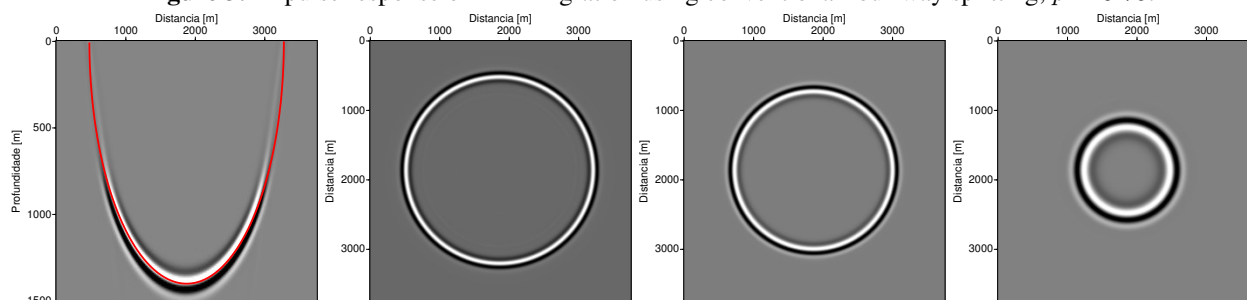

Figure 4: Impulse response of FFD migration using alternating four-way splitting; $p = 0.75$.

Padé approximation. Note that the observed behaviour will be emphasized in media with strong lateral variations, where much smaller values of p will occur.

Figure 3 shows the impulse response of FFD migration using conventional four-way splitting. The circular shape of the impulse-response has been nicely recovered by the application of the two additional differential operators in the diagonal directions. Also, the amplitude loss in the coordinate directions is no longer visible. Note that this image has about twice the computational cost of the one in Figure 4.

Figure 4 shows the impulse response of CPFFD migration using alternating four-way splitting, i.e., two-way splitting in the coordinate directions at one depth level and in the diagonal directions at the next depth level. It is hard to spot any difference to the result of complete four-way splitting of Figure 3. The circular format of the operator is almost perfect, and even the slight amplitude loss along the coordinate axes is as well recovered as by complete four-way splitting. Note that this image has about the same computational cost as the one obtained with conventional two-way splitting of Figure 2.

Figure 5 shows the impulse response of FFDPI migration using conventional two-way splitting, with interpolation between wavefields obtained for $p = 0.9$ and $p = 1.1$. We chose these values to reflect the fact that for FFDPI, generally reference velocities closer to the medium velocity are available for interpolation. We observe a good preservation of the circular shape, particularly in the horizontal cuts. In the vertical cut, we note that the wavefront lags slightly behind the true position, starting already at rather low propagation angles of about $35°$. The amplitude decay for high propagation angles is reduced as compared to FFD, probably because the reference velocities are closer to the medium velocity than in the previous examples. Finally, the shallowest cut exhibits some numerical dispersion, causing a distorted pulse shape.
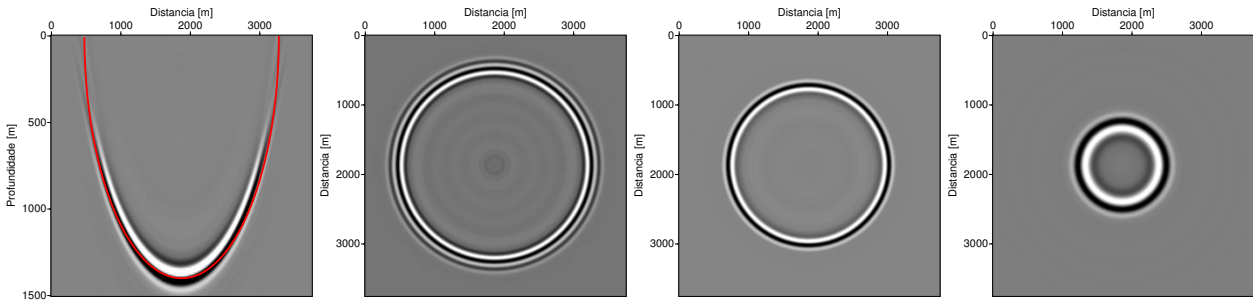
Figure 5: Impulse response of FFDPI migration using conventional two-way splitting, with interpolation between $p = 0.9$ and $p = 1.1$.
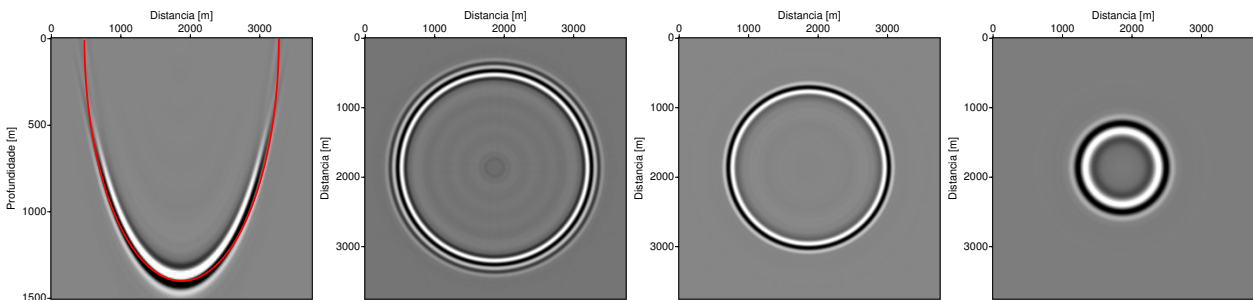

Figure 6: Impulse response of FFDPI migration using alternating four-way splitting, with interpolation between $p = 0.9$ and $p = 1.1$.

Figure 6 shows the impulse response of FFDPI migration using alternating four-way splitting, with interpolation between wavefields obtained for $p = 0.9$ and $p = 1.1$. Almost no improvement over the conventional two-way splitting result of Figure 5 is visible.

Tests in an inhomogeneous medium

For a more realistic test of the different splitting techniques for FFD migration, we calculated zero-offset impulse responses for the EAGE/SEG salt model. Here, we used a seismic pulse in the centre of the model, described by a Ricker wavelet with central frequency of 15 Hz, dislocated by $t_e = 1.1$ s, and a migration grid with $\Delta x = \Delta y = \Delta z = 20$ m. To avoid spurious events from the spike reflectors, we regularized the model using a 7×7 median filter.

We represent the results by vertical cuts parallel to the y-z plane at $x = 4.14$ km and $x = 6.80$ km, and parallel to the x-z plane at $y = 4.14$ km and $y = 10.22$ km, as well as horizontal cuts at depths $z = 1.7$ m, $z = 2.9$ km, $z = 3.5$ km, and $z = 4.1$ km. Figures 7 and 8 show these cuts through the EAGE/SEG salt model after filtering.

Figures 9 and 10 show the corresponding cuts through the impulse response of FFD migration with two-way splitting, and Figures 11 and 12 those of FFD migration with alternating four-way splitting. The differences between these sets of figures are due to numerical anisotropy, which is not always easy to see at this scale. The most visible difference is the one between the top left images of Figures 10 and 12. The circular shape of three quarters of the wavefront is well preserved in Figure 12, while visibly distorted in Figure 10. Similar distortions are present in the other figure parts. Some events, particularly in the diagonal directions, are slightly more advanced in Figures 11 and 12 than in Figures 9 and 10. Also, some amplitude differences are visible. We refrain from presenting the results of complete four-way splitting, because they look virtually identical to those in Figures 11 and 12.

For comparison, Figures 13 and 14 show the impulse response of FFDPI migration with two-way splitting. Since the theory of Biondi (2002) is only formulated for a single term of the Padé series, so is our implementation. Because of the strong dependence of FFDPI on reference velocities not too far from the true model velocity, this numerical experiment needed 10 reference velocities. For being a very robust
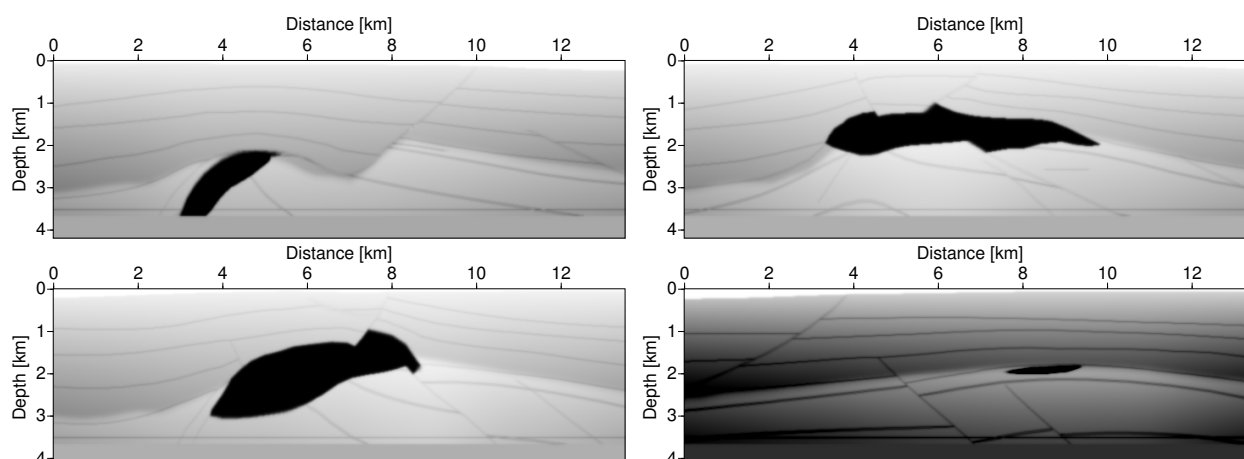
Figure 7: EAGE/SEG salt model. Representation by 4 vertical cuts at $x = 4.14$ km, $x = 6.80$ km (top), $y = 4.14$ km, and $y = 10.22$ km (bottom).
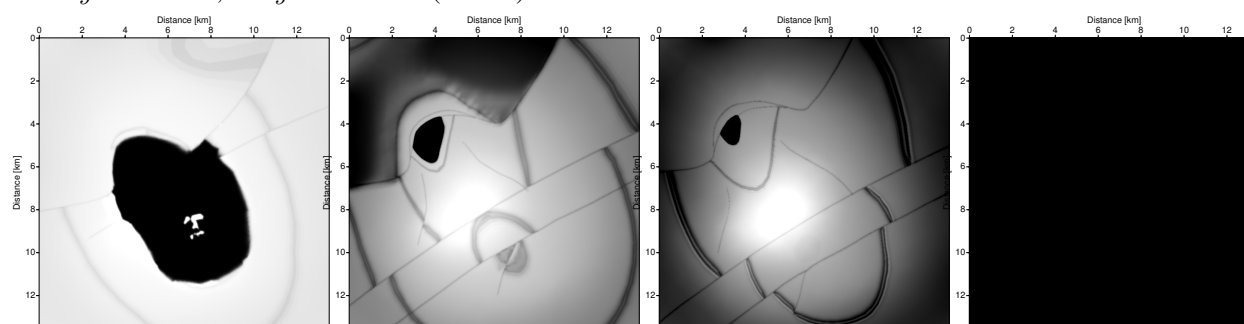

Figure 8: EAGE/SEG salt model. Representation by 4 horizontal cuts at $z = 1.7$ km, $z = 2.9$ km, $z = 3.5$ km, and $z = 4.1$ km (from left to right).

method, the impulse response is not subject to any instabilities, even with the reference velocities being still a bit far from the medium velocities. This remains true even for less reference velocities, though the image quality degrades considerably. Because of the need for a rather large number of reference velocities, FFDPI is a rather expensive method. In our implementation, it used about three times the computational time of alternating four-way FFD.

Even for this experiment with 10 reference velocities, we still see some effects of numerical dispersion in Figures 13 and 14. Also, the results still exhibit quite visible differences to Figures 11 and 12. Since we have at this time no 3D reverse-time migration available, it is hard to tell which results are better positioned. Visual inspection and comparison to results of FD migration (not shown here) make us believe that the FFD results are more reliable than the FFDPI results with 10 reference velocities. More accurate results can be obtained by further increasing the number of reference velocities.

CONCLUSIONS

In this paper, we have implemented 3D versions of complex Padé FFD (CPFFD) and FFD plus interpolation (FFDPI), which have proven to be more stable in the presence of strong lateral velocity contrasts than other FFD migration implementations. For CPFFD migration, we have compared the effects of different ways of directional splitting and compared its results to those of FFDPI migration. Alternating four-way splitting, i.e., applying the differential operators in the coordinate directions at one depth level and in the diagonal directions at the next depth level, proved to be an improvement over conventional two-way splitting at almost no extra cost. The results were comparable to complete four-way splitting, i.e., all four directions applied at all depth levels. Extensions of the alternating splitting technique can be thought of like eight-way splitting where the remaining directions are covered two by two in the next two depth steps.

From our numerical tests with splitting the CPFFD and FFDPI migration operators, we conclude that FFDPI migration is the most robust of the tested methods. Even implemented only using two-way splitting,
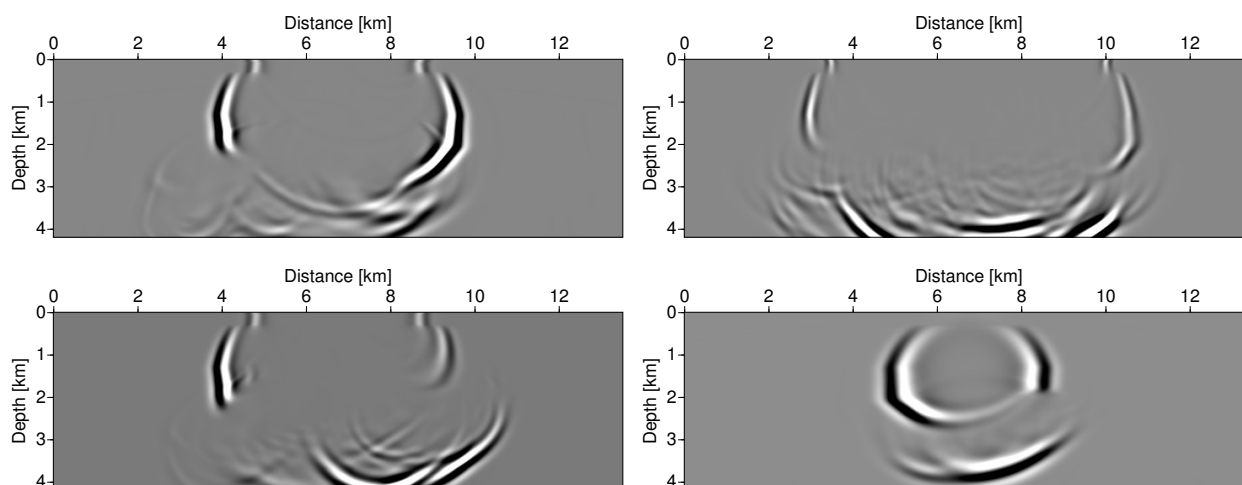
Figure 9: Impulse response of FFD migration with two-way splitting. Cuts as above.
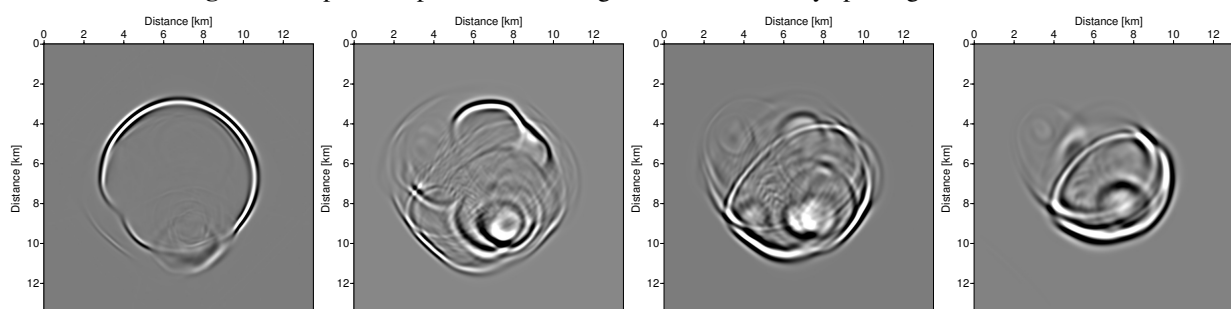

Figure 10: Impulse response of FFD migration with two-way splitting. Cuts as above.

it did show only a fair amount of numerical dispersion, but no visible numerical anisotropy. However, for practical use, FFDPI is a rather expensive method because it needs a large number of reference velocities to function with acceptable precision. Thus, for a more economic migration with acceptable image quality, alternating four-way splitting in FFD migration is an interesting alternative.

One minor problem of multi-way splitting should be mentioned. The differential operator in the diagonal directions can cause aliasing effects because of the fact that the grid spacing in this direction is by a factor of $\sqrt{2}$ larger than in the coordinate directions. Off-diagonal directions may complicate things further, because they require resampling.

REFERENCES

Amazonas, D., Costa, J. C., Schleicher, J., and Pestana, R. (2007). Wide-angle FD and FFD migration using complex Padé approximations. *Geophysics*, 72(6):S215–S220.

Bamberger, A., Engquist, B., Halpern, L., and Joly, P. (1988). Higher order paraxial wave equation approximations in heterogeneous media. *J. Appl. Math.*, 48:129–154.

Biondi, B. (2002). Stable wide-angle Fourier finite-difference downward extrapolation of 3-D wavefields. *Geophysics*, 67(3):872–882.
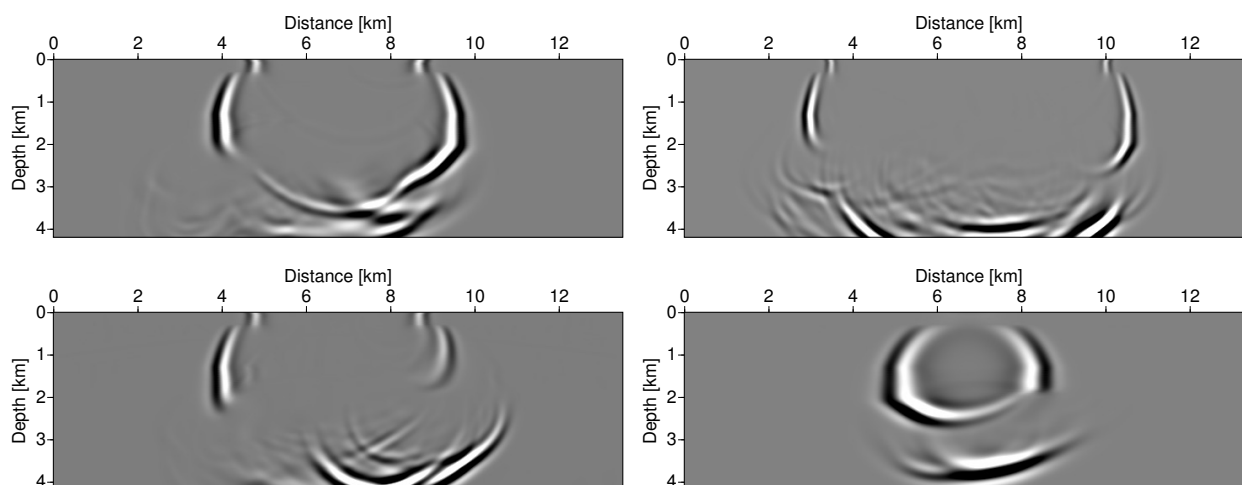
Figure 11: Impulse response of FFD migration with alternating four-way splitting. Cuts as above.
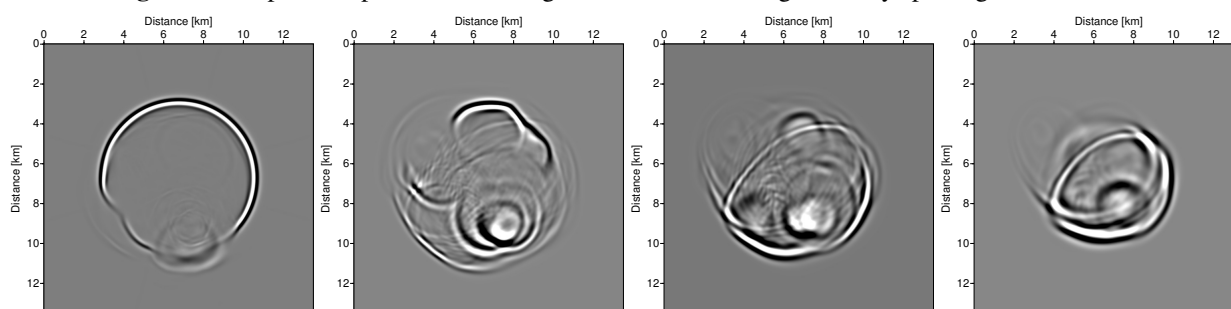

Figure 12: Impulse response of FFD migration with alternating four-way splitting. Cuts as above.

Brown, D. (1979). Muir's rules for matrices: Another look at stability. *Stanford Exploration Project Report*, SEP-20:125–142.

Brown, D. L. (1983). Applications of operator separation in reflection seismology. *Geophysics*, 48:288–294.

Claerbout, J. F. (1971). Toward a unified theory of reflector mapping. *Geophysics*, 36(3):467–481.

Collino, F. and Joly, P. (1995). Splitting of operators, alternate directions and paraxial approximation of the 3D wave equation. *SIAM Journal on Scientific Computing*, 16:1019–1048.

Douglas, J. (1962). Alternating direction methods for three space variables. *Numerische Mathematik*, 4:41–63.

Gazdag, J. and Sguazzero, P. (1984). Interval velocity analysis by wave extrapolation. *Geophys. Prosp.*, 32(03):454–479.

Godfrey, R. J., Muir, F., and Claerbout, J. F. (1979). Stable extrapolation. *Stanford Exploration Project Report*, SEP-16:83–87.

Graves, R. W. and Clayton, R. W. (1990). Modeling acoustic waves with paraxial extrapolators. *Geophysics*, 55:306–319.

Jin, S., Wu, R. S., and Peng, C. (1999). Seismic depth migration with pseudo-screen propagator. *Computational Geosciencies*, 3:321–335.

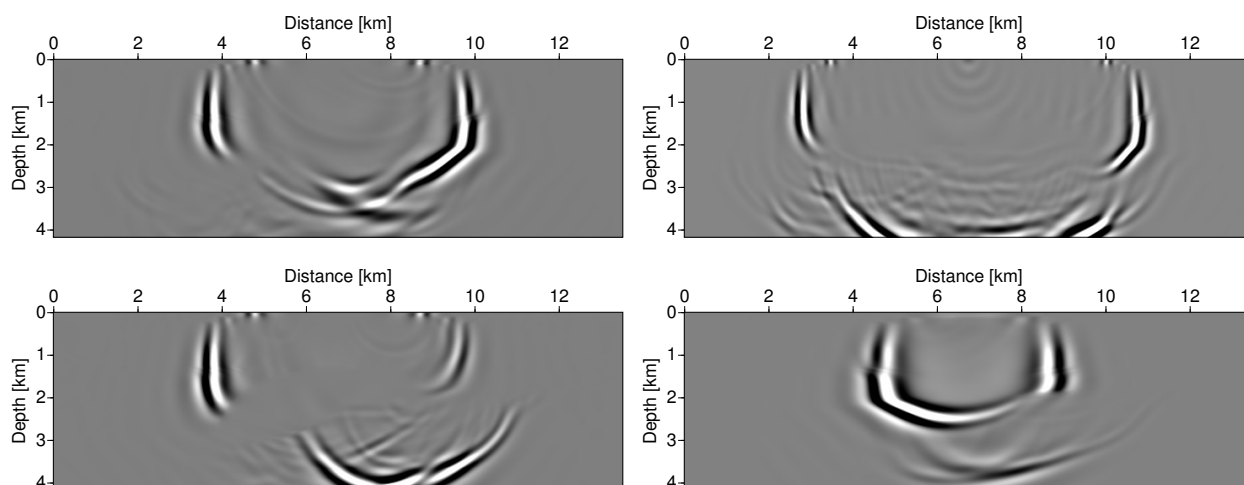Kessinger, W. (1992). Extended split-step Fourier migration. *SEG, Expanded Abstracts*, 11(1):917–920.

Figure 13: Impulse response of FFDPI migration with two-way splitting using 10 reference velocities. Cuts as above.
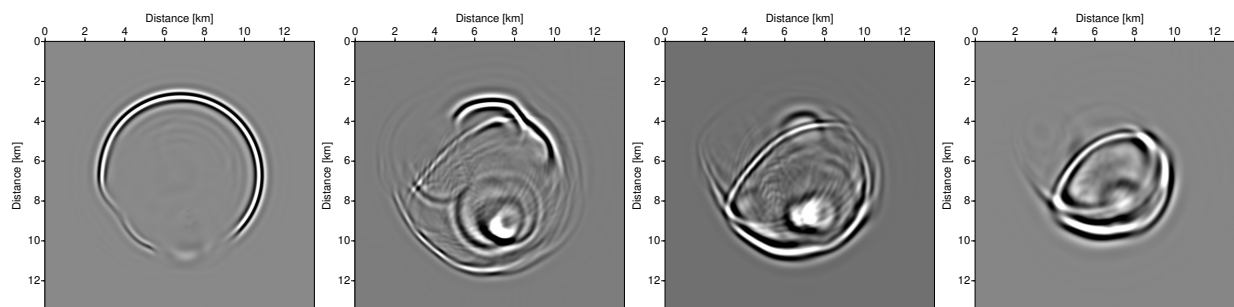

Figure 14: Impulse response of FFDPI migration with two-way splitting using 10 reference velocities. Cuts as above.

Kitchenside, P. (1988). Steep dip 3-D migration: Some issues and examples. In *58th Annual International Meeting, SEG, Expanded Abstracts*, pages 976–978.

Leontovich, M. A. and Fock, V. A. (1946). Solution of the problem of propagation of electromagnetic waves along the earth's surface by the method of parabolic equation. *Journal of Experimental and Theoretical Physics*, 16:557–573.

Li, Z. (1991). Compensating finite-difference errors in 3-D migration and modeling. *Geophysics*, 56(10):1650–1660.

Millinazzo, F. A., Zala, C. A., and Brooke, G. H. (1997). Square-root approximations for parabolic equation algorithms. *Journal of the Acoustical Society of America*, 101(2):760–766.

Mitchell, A. R. and Griffiths, D. F. (1980). *The finite difference method in partial differential equations*. Wiley.

Ristow, D. (1980). *3-D downward extrapolation of seismic data in particular by finite difference method*. PhD thesis, University of Utrecht.

Ristow, D. and Rühl, T. (1994). Fourier finite-difference migration. *Geophysics*, 59(12):1882–1893.

Ristow, D. and Rühl, T. (1997). 3D implicit finite-difference migration by multiway splitting. *Geophysics*, 62:554–567.

Wachspress, E. L. and Harbetler, G. J. (1960). An alternating-direction-implicit iteration technique. *SIAM Journal*, 8:403–424.

Wang, Y. (2001). ADI plus interpolation: Accurate finite-difference solution to 3D paraxial wave equation. *Geophysical Prospecting*, 49:547–556.

Wapenaar, C. P. A. (1990). Representation of seismic sources in the one-way wave equation (short note). *Geophysics*, 55(06):786–790.

Xie, X. R. and Wu, R. S. (1998). Improve the wide angle accuracy of screen method under large contrast. pages 1811–1814.

Zhang, G. Q., Zhang, S. L., Wang, Y. X., and Liu, C. Y. (1988). A new algorithm for finite-difference migration of steep dips. *Geophysics*, 53:167–175.

Zhou, H. and McMechan, G. A. (1997). One-pass 3-D seismic extrapolation with the 45° wave equation. *Geophysics*, 62:1817–1824.